Oday A. Hammadi [1]
Mohammed K. Khalaf [2]
Firas J. Kadhim [3]
Bahaa T. Chiad [3]

[1] *Department of Physics, College of Education, Al-Iraqia University, Baghdad, IRAQ*
[2] *Ministry of Science and Technology, Baghdad, IRAQ*
[3] *Department of Physics, College of Science, University of Baghdad, Baghdad, IRAQ*

Key Mechanisms of Low-Pressure Glow Discharge in Magnetized Plasmas

In this article, the key mechanisms of glow discharge in low-pressure gas mixtures were presented and discussed. The particle motions – mainly collisions – in discharge plasma those considered in most applications of plasma were presented. The regions of glow discharge were identified and their main characteristics were highlighted. These mechanisms were supported by experimental results obtained from a homemade dc plasma sputtering system. The experimental parameters, such as inter-electrode distance, using magnetrons and adding nitrogen to the gas mixture, and their effects on the Paschen's curve of glow discharge were introduced.

Keywords: Glow discharge; Particle motion; Magnetron plasma; Low-pressure plasma

1. Introduction

The motion of a charged particle under the influence of electric and magnetic fields is described by Lorentz force equation as [1]

$$\vec{F} = m\frac{d\vec{v}}{dt} = q\left(\vec{E} + v \times \vec{B}\right) \quad (1)$$

where $\vec{F}$ is the force acting on a particle of charge q and velocity v in the presence of electric field ($\vec{E}$) and magnetic field ($\vec{B}$)

According to this equation, a particle of positive charge will be accelerated along the direction of the electric field while a particle of negative charge will be accelerated in opposite direction of the electric field. However, each of them will move in circular path around a guiding center in a plane perpendicular to the magnetic field, i.e., both particles will drift in the same direction and the same velocity [1-3]. The combination of both motions results in a total motion referred to as "Hall drift velocity" ($v_{E/B}$) and directed perpendicular to both electric and magnetic fields, as shown in figure (1).

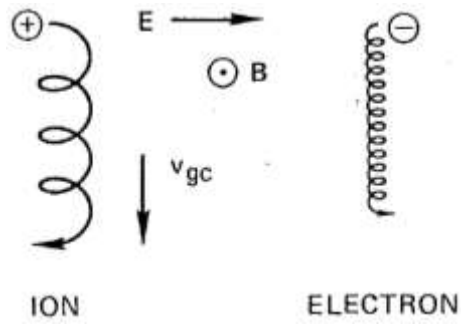

Figure (1) Single particle motion in combined electric and magnetic fields [1]

The radius of this gyration motion is known as Larmor radius, whose value is roughly about 1mm for an electron and on the same scale as vacuum chamber (tens of centimeters) for an ion [4]. The electrons are well confined in the plasma due to their small gyration radii while ions have much larger gyration radii, so they can, more or less, freely cross the magnetic field lines and hence; are weakly confined [5].

In plasmas employed for physical vapor deposition (PVD), plasma dynamics consist of more than Hall drift as the most important drifts are the curved magnetic vacuum field gyro drift ($v_{e,R}$) and pressure gradient (or diamagnetic) drift ($v_{e,\nabla p}$) [6-9]. They are given by

$$v_{e,R} = \frac{2k_B T_e}{e}\frac{R_c \times B}{R_c^2 B^2} \quad (2)$$

$$v_{e,\nabla p} = \frac{\nabla p \times B}{e n_e B^2} \quad (3)$$

here R_c is the radius of curvature of the magnetic field lines and ∇p is the pressure gradient

All three drift contributions are of significant amplitude and in the same direction, therefore, a net force on the electrons is resulted to move them away from the cathode.

In the same way that electric fields affect the behaviors of charged particles in gas discharge plasma, magnetic fields cause charged particles to behave differently by changing their directional vectors by an amount proportional to the magnetic field strength and gradient. Accordingly, using magnetic fields – in conjunction with electric fields – is employed to establish closed plasma configurations contained in limited volume [10].

The discharge of gas is composed of different particles such as electrons, ions, neutral atoms and photons [11]. In a discharge of gas, inelastic collisions are the dominant where the kinetic and potential energies of the colliding particles are changed. However, elastic collisions are occurring and involving electron scattering as the electron changes its direction but its kinetic energy after the collision is same as before collision [12].

The collision between the electron and neutral atom in gas discharge is the most important and frequent collision of particles since this collision is

 ISSN (printed) 1813-2065, (online) 2309-1673 Printed in IRAQ

responsible of maintaining the discharge by the continuous ionization of neutral atoms by electrons [13-15]. In this collision process the primary electron removes a bound electron on an atom producing a positive ion and two electrons. These electrons are then accelerated through an electrical field generating further ionization [16].

If a photon collides with a neutral atom in the ground state or with atoms at the wall of the vacuum chamber, ionization can also occur and is known as photoionization [17]. When an electron possesses sufficient energy to displace a bound electron of an atom to higher orbit, this atom will be excited by a process known as excitation and remain in the excited state for period of time about 10^{-8} second before the displaced electron returns to its original orbit and emits the energy difference between two orbits as a radiation (photons). This emission process is the origin of the glow characteristics of a gas discharge [18]. Obviously, the energy required for excitation is less than that required for ionization because the electron of an excited atom is not removed completely from this atom. For example, the excitation energy of argon atoms is 11.6eV while the ionization energy is 15.7eV [19]. As well, the excitation energy must be greater than or equal to the energy of the electronic state in order for the excitation to occur. Table (1) presents the excitation and ionization energies levels for various elements.

Table (1) Excitation and ionization energy levels for various elements [19]

Element	Excitation energy (eV)	Ionization energy (eV)
Hydrogen	10.2	13.6
Helium	20.91	24.58
Nitrogen	6.3	14.54
Argon	11.5	15.7
Aluminum	3.13	5.98

There are certain energy levels corresponding to particular orbits to which an electron may be displaced but from which it cannot easily return to its original level. So, the atom may remain in this excited metastable state for a long time (1-1000) milliseconds [20]. Due to long lifetimes, atoms at excited metastable states may receive – with a relatively high probability – sufficient energy from subsequent electron collisions to get ionized [21].

A neutral gas atom can possibly be ionized by a collision with another atom in a metastable state. This process is known as Penning ionization, which leads the atom in the metastable state to return to its ground state [22]. As well, when two atoms in the metastable states collide with each other, ionization may occur. However, the major ionization of atoms in the metastable states is caused by the collisions with electrons as the energy required is only 27% of ionization energy as in argon gas [23]. Some reaction mechanisms in gas discharge are given below

(a)	$A^+ + A^+$	→	$A + A^{++}$	Ion-Ion
(b)	$A^+ + B$	→	$B^+ + A$	Ion-Neutral
(c)	$A^+ + A$	→	A_2^+	Ion-Neutral
(d)	$e^- + e^-$	→	$e^- + e^-$	Electron-Electron
(e)	$e^- + A^+$	→	$A^{++} + 2e^-$	Electron-Ion
(f)	$e^- + A$	→	A^-	Electron-Atom
(g)	$e^- + A^*$	→	$A + e^-$	Electron-Atom (excited)
(h)	$e^- + A$	→	$A^* + e^-$	Electron-Atom
(i)	$e^- + A$	→	$A^- + h\nu$	Electron-Atom
(j)	$h\nu + A^-$	→	$A + e^-$	Photon-Ion

It is well known that gas discharge can be generated when an electric field is applied between two electrodes at sufficient separation in the presence of a gas. The excitation of an orbital electron to a higher state with subsequent decay to the ground state with the emission of photons is resulted from many electron-atom collisions, so, there is a considerable light emitted by the discharge [24]. Figure (2) shows the representations of the structure of a glow discharge in a dc diode system. Light intensity, potential distribution, electric field strength, net space charge, negative charge distribution and positive charge distribution, are explained before [25].

First region in gas discharge is called “cathode glow”, which is a thin sheet of very high luminosity and in contact with the cathode surface. There are two possible types of glow. One possibility is associated with the electrons ejected from the cathode surface as a result of the interaction between the incident ions and the lattice electrons [26]. The electrons from the surface have low energies and experience collisions with the gas atom near the cathode surface and cause excitations. The second possibility is due to the neutralization of Ar ions which may gain an orbital electron in an excited state of an atom and in decaying to the ground state will emit a photon [27].

The next region is called “cathode dark space” or “Crookes dark space”. It shows much lower luminosity than the cathode glow due to the lack of excitations and emissions of photons since no electron-atom collisions occur in this region [28]. The secondary electrons emitted from the cathode are accelerated through the high electric field in this zone with a very high velocity characterized by their low mass. There is an abundance of ions in the dark space mainly due to the negative voltage applied to the cathode, which has driven out the lighter, easily influenced electrons due to the field strength at the electrode. As the mobilities of ions are very much lower than those of electrons, the net space charge in this region is positive [29].

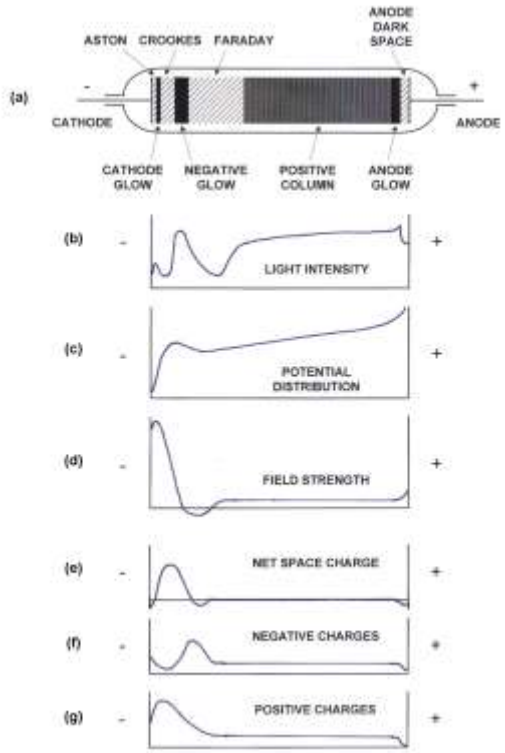

Figure (2) Representations of the (a) structure of a glow discharge in a dc diode system (b) light intensity, (c) potential distribution, (d) electric field strength, (e) net space charge, (f) negative charge distribution and (g) positive charge distribution [26]

The result is the screening of the cathode by a cloud of positive ion species, which ensures that almost all of applied voltage falls off across this dark space. This means that only a small potential drop remains across the remainder of the tube. This large voltage drop is the acceleration mechanism for the ions that enter the dark space by diffusion from the negative glow region. This is the basic process of sputtering which ensures that the glow is sustained by the production of secondary electrons emitted from the cathode [30]. These accelerated ions are also neutralized at the cathode and these liberated electrons (typically 1 electron per 10 ions, i.e., 0.1) are quickly repelled by the electric field and maybe involved in the ionization processes with neutral gas atoms if their energies are sufficient to cause inelastic collisions. The combined results of these ionization effects are seen as the next region (negative glow) [31].

As electrons are slowed down in the dark space, they immediately gain a high acceleration by the electric field. Soon these electrons reach the end of the dark space, they enter the negative glow regions, in which they collide and ionize the neutral gas atoms at distances corresponding to their mean free paths. Consequently, this region is the most luminous one in the discharge [15]. Most electrons give up a great amount of energy due to the collisions with neutral atoms even before they have passed through the region. Consequently the electric field in the negative glow decreases [16].

The end of the negative glow corresponds to the range of electrons with sufficient energy to produce excitation. The sustaining feature of a bombarding ion recombining with an electron at the cathode also ensures overall net zero charge as the liberated electron causes ion generation to balance. The cathode glow is the result of this recombination at the cathode surface [17].

The next region is called “Faraday dark space”. It is much less luminous and includes approximately zero electric field strength because the electrons reaching it have already given up most of their energies; therefore, they have too little energies to cause further excitation of the neutral atoms [18].

The final region is called the “positive column”. It is the ionized region extending from the Faraday dark space almost to the anode and serving merely as a conduction path between them. This region is known as the plasma, as the net charge in this column is near or at zero. Electrons that gain enough energy in the last few mean free paths to excite ions being accelerated from the anode glow region [19]. Most of the probe investigations and substrate placement are made in the positive column [20].

2. Experimental Part

The magnetron sputtering system used in this work was designed to include vacuum chamber, discharge electrodes and magnetron assembly, vacuum unit, dc power supplies, gas supply system, cooling system and measuring instruments. The system is schematically shown in figure (2).

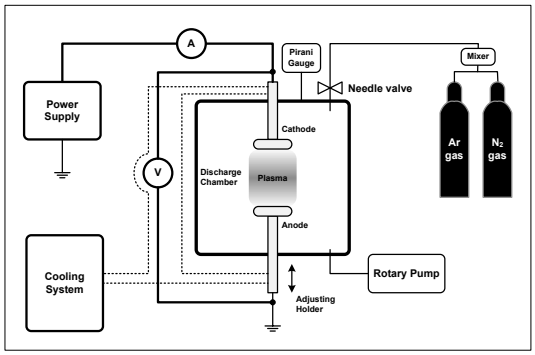

Figure (2) Schematic diagram of the system used in the present work

The vacuum chamber was constructed from stainless steel. It is a cylinder with internal diameter of 35cm, outer diameter of 45cm, and height of 37.5cm. There were four side holes of 10.8cm in diameter on the circumference of the cylinder; one of them was closed with a quartz window, while the other three were closed with glass windows. These windows were mounted by stainless steel flanges each of 21cm in diameter and four screws. They were used for monitoring the discharge and events inside the chamber. Each window was far from the

 ISSN (printed) 1813-2065, (online) 2309-1673 Printed in IRAQ

discharge region by a neck of 7.5cm diameter to avoid the effects of heat developed by the glow discharge.

The vacuum chamber was sealed from lower end with a stainless steel flange of 40cm in diameter containing a feedthrough for electrical connections required for experiment. The upper end was sealed with a similar flange but containing two feedthroughs; one for gas inlet and Pirani gauge and the other for the Penning gauge. Both flanges include a central hole for the electrode hollow holder. Rubber O-rings and silicon vacuum grease were used in all sealing points.

Both discharge electrodes were constructed from stainless steel (St. St. 304) hollow disks of 80mm in diameter and 8.5mm in thickness. The electrode was joined to holder of 295mm in length and outer and inner diameters of 16.2mm and 11.6mm, respectively, to include a stainless steel channel of 78.5mm in length and 5.6mm in diameter through which the cooling water was flowed to the inside volume of the electrode. The holder tube includes a 1mm-step screw thread of 25.88mm in length to connect the cooling channel tightly.

Two permanent ring magnets were placed at the back side of each electrode to form the magnetron, as shown in figure (3), with a separating distance of 1cm. The inner magnet was 12.5mm in height and 31.5mm in diameter with a central hole of 17.5mm in diameter, while the outer magnet was 15.2mm in height and 80mm in diameter with a central hole of 40mm in diameter. Therefore, the two magnets were separated by a distance of 10mm around their opposing surfaces. A metallic disk of 69.7mm in diameter and 2.5mm in thickness was used to choke the outer magnet to prevent the magnetic field lines from extending to the backside of the electrode.

The design of dual magnetrons proposed in this work provides two concentric regions of high magnetic field intensity on electrode surface. At these regions, the charged particles are totally confined because the particles escaping from the inner region towards the walls of vacuum chamber will lose some energy and then be trapped by the outer region. In conventional configurations, a fraction of charged particles can escape from the confinement region and hence decrease the ionization rate near the cathode.

The advantage of magnetron on the anode is observed in the film deposition of ferromagnetic materials because the magnetic field intensity forces the deposited particles to distribute on the substrate according to its distribution. This makes possible to produce films with selective optical densities to serve multipurpose devices as in the optical data storage applications [32].

In order to prevent any variation in the arrangement of internal components, a teflon host of 100mm diameter and 44.5mm height with a central groove of 84.75mm diameter and 26.3mm depth was used to maintain the magnetron from the backside of the electrode. This piece was locked from movement by cylindrical teflon piece of 37.5mm in diameter and 35.25mm in height containing an M5 screw driven towards the holder tube.

A single-stage rotary pump (Leybold-Heraeus) of 9 m^3/hr pumping speed was used to get pressure down to about 10^{-3} mbar inside the vacuum chamber. A water-cooled diffusion pump was available for use in this work for lower vacuum pressure and connected to the vacuum chamber via a trap. However, all results presented were obtained using the rotary pump only as vacuum pressure of 10^{-2} mbar was easily reached. The minima of Paschen's curves for the inter-electrode distances 2-6 cm were achieved at pressures higher than 10^{-3} mbar. Pirani gauge (down to 10^{-3} mbar) was used. The flow rate of the Ar:N_2 mixture was ranging between 20-50 cm^3/s.

The electrical power required for generating discharge inside vacuum chamber was provided by a 5 kV dc power supply (Edwards 2A) through high-tension cables. A current-limiting resistance (3.25 kΩ, 1 kW) was connected between the negative terminal of the dc power supply and the cathode inside the vacuum chamber, while the positive terminal of the dc power supply was connected directly to the anode. The output voltage of the power supply could be varied precisely over 0-5 kV to control the current flowing between discharge electrodes. However, the maximum supply voltage did not exceed 800V. Another dc power supply (0-250 V PHYWE-7532) was used to provide bias potential for Langmuir probe measurements. In addition, a third dc power supply (DHF-1502DD, 1.5-15V, 0.6-2A) was used for electrical measurements performed on the samples prepared as photodetectors.

Gas supply unit consists of argon and nitrogen cylinders, flowmeters, gas flow regulators, needle valves and connections and joints. Argon gas of 96% purity and nitrogen gas of 90% purity were used.

A compact unit was used to cool and circulate the room-temperature water through a channel in discharge electrodes. This unit can cool more than 51 liters of distilled water down to about 4°C and circulate it with maximum flow rate of 30 L/min. The temperature inside the chamber was measured by a thermometer located near the wall of the chamber while the temperatures of both electrodes were measured by thermocouples connected to digital instruments. The maximum surface temperature of the substrate placed on the anode was 40-45°C with uncooled circulating water and reasonably reduced with cooled circulating water.

The operating conditions of the system were classified into two groups; constant and variable. The constant operating conditions include inter-electrode distance, vacuum pressure, current limiting resistance, discharge voltage, discharge current,

cooling temperature, cooling water flow rate and deposition time. The variable operating conditions include gas pressure and gas flow rate. Varying discharge voltage was almost possible during the operation. In addition, turning the cooling system off would raise the temperature of either electrode to 40-45°C with circulating water, while stopping the circulation of water would raise electrode temperature more (up to 150°C).

Results and Discussion

As mentioned before, Paschen's curve is one of the most characteristics of gas discharges as it describes the region at which the required application of gas discharge is effectively determined.

In figure (4), the Paschen's curve of argon gas discharge – without magnetrons at the electrodes – was plotted at different inter-electrode distances (2-6cm) in order to determine the point at which the sputtering process is applicable. As seen, in the left-hand side of the curve, the breakdown voltage increases with decreasing gas pressure and inter-electrode spacing. These results can be explained as a decrease in the collision frequency. At low gas pressure, the electron mean free path was longer and collision probability was less than that at high gas pressure, so there were few collisions. There is low probability that any of the secondary electrons emitted can collide with neutral atoms during the journey from the cathode to the anode. In the right-hand side, the breakdown voltage increases slowly with the increase of gas pressure, i.e., the ionization cross-section increases, with the increase of *p.d* product. Therefore, electrons need more energy to ionize the neutral atoms.

As shown in figure (4), at inter-electrode distances of 2, 3 and 4cm, the Paschen's curve are approximately coincided and the minima of *p.d* product are 1, 1.05 and 1 mbar.cm, at breakdown voltages of 185, 189 and 190V, respectively.

At inter-electrode distances of 5 and 6cm, the minimum points are shifted towards higher values (1.25 and 1.5mbar.cm), which are not applicable in sputtering applications. This can be attributed to the higher voltages required for breakdown at larger distances. Apparently, such a shift of the breakdown curves toward higher values of V_B and *p.d* with increasing distance (*d*) may be attributed to an increase in losses of charged particles on the cylindrical wall of the discharge tube. This is due to diffusion across the electric field.

In order to explain the effect of using magnetrons at the electrodes, the Paschen's curve was plotted at certain inter-electrode distance (2, 4 and 6cm) for three different cases (without magnetrons, with one magnetron at the cathode, and with dual magnetrons), as shown in figure (5).

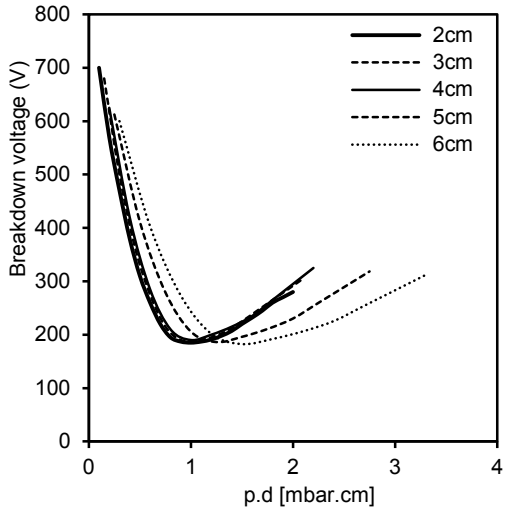

Figure (4) Paschen's curves of argon gas discharge at different inter-electrode distances (2-6cm) without magnetrons at the electrodes

In figure (5a), the effect of using only one magnetron at the cathode is small when compared to the case of dual magnetrons used. In figure (5b), the effect of using magnetrons is reasonably clear. In figure (5c), the effect of using magnetrons is absent in the left part of the curve as it appears clearly in the right part of it.

Paschen's curve was plotted for the argon:nitrogen mixture (4:1) and compared to that obtained for argon gas at inter-electrode distance of 4cm using dual magnetrons, as shown in figure (6). This curve was clearly shifted upward due to the presence of nitrogen molecules in the gas mixture and they require relatively high voltages for breakdown (V_{min}~240V). Accordingly, the $(p.d)_{min}$ point was shifted downward to about 0.8 mbar.cm.

One of the important characteristics of gas discharges is the relation of discharge current with the working gas pressure.

The variation of discharge current with working gas pressure at certain discharge voltage (700V) and different inter-electrode distances is plotted as shown in figure (7). First, the discharge current is rapidly increasing (up to 46mA) with small increase in working gas pressure. During the variation of working gas pressure from 1 to 3 mbar, the variation in discharge current is small (1-4%). The discharge current is decreasing with increasing gas pressure above 3mbar. And this behavior of discharge current with working gas pressure is explained as follows; this relation was plotted at certain discharge voltage of 700V and three certain distances between the electrodes when no magnetrons are used, when only one magnetron is used at the cathode, and when dual magnetrons are used, as shown in figures (8).

 ISSN (printed) 1813-2065, (online) 2309-1673 Printed in IRAQ

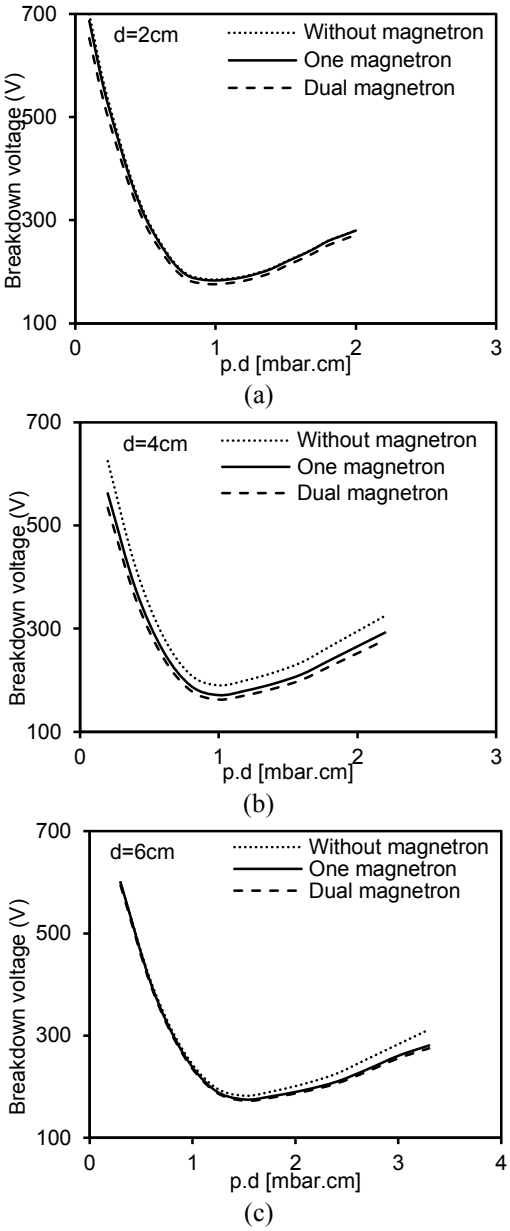

Figure (5) Paschen's curves of Ar gas discharge at working gas pressure of 0.7mbar and inter-electrode distances of (a) 2cm, (b) 4cm and (c) 6cm for three different cases (without magnetrons, with one magnetron at the cathode, and with dual magnetrons)

At inter-electrode distance of 4cm and discharge voltage of 700V, the relation between discharge current and argon/nitrogen mixture (4:1) pressure was plotted and compared to that for only argon, as shown in figure (9). Higher current was measured as the production of the charged particles was increased due to the additional contributions from ionized nitrogen molecules.

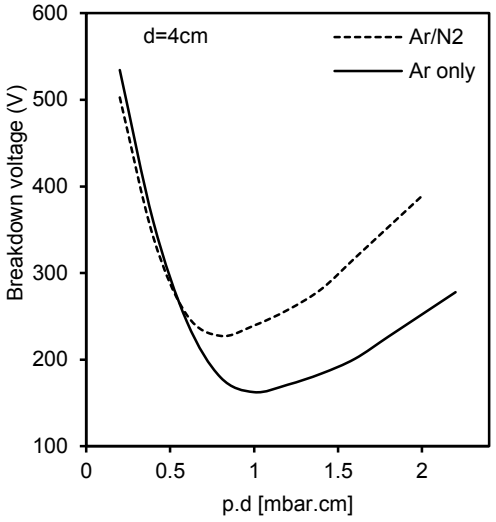

Figure (6) Comparison of Paschen's curves for argon gas and argon/nitrogen mixture (4:1) discharges at inter-electrode distance of 4cm with dual magnetrons

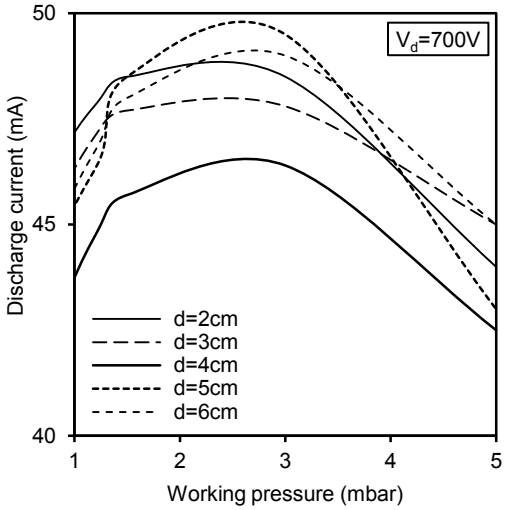

Figure (7) Variation of discharge current with working Ar gas pressure at V_d=700V and different inter-electrode distances without magnetrons at the electrodes

As the density of particles (Ar atoms and N_2 molecules) in discharge volume is increased, the mean free paths of electrons are reduced and their collisions with argon atoms and nitrogen molecules are accordingly increased. So, an electron in case of argon/nitrogen mixture may make more collisions than in case of argon only and hence produce more ions. These ions may include argon and nitrogen ions, as the former are employed for sputtering while the latter are required for silicon nitride formation.

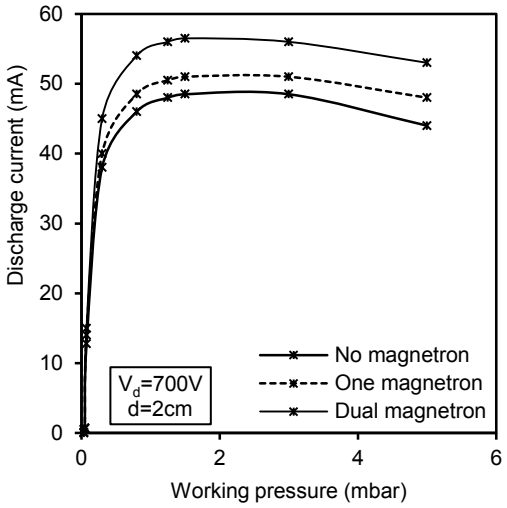

(a)

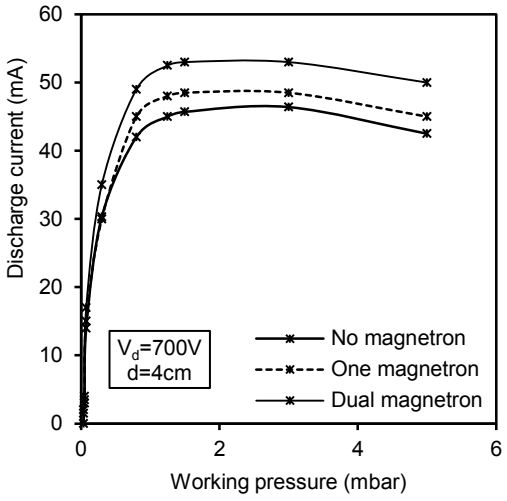

(b)

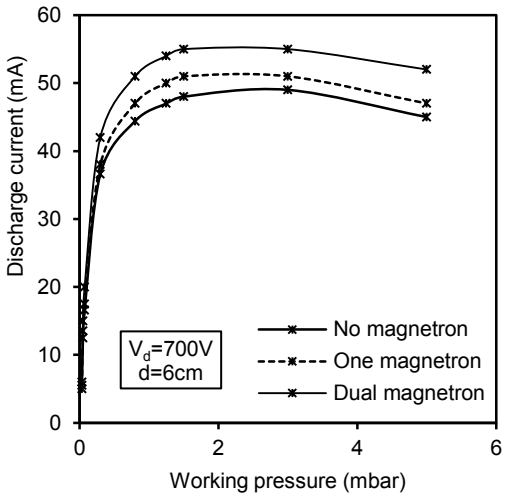

(c)

Figure (8) Variation of discharge current with working gas pressure (Ar) for three different cases (without magnetrons, with one magnetron at the cathode, and with dual magnetrons) at discharge voltage (700V) and different inter-electrode distances (a) 2cm, (b) 4cm, (c) 6cm

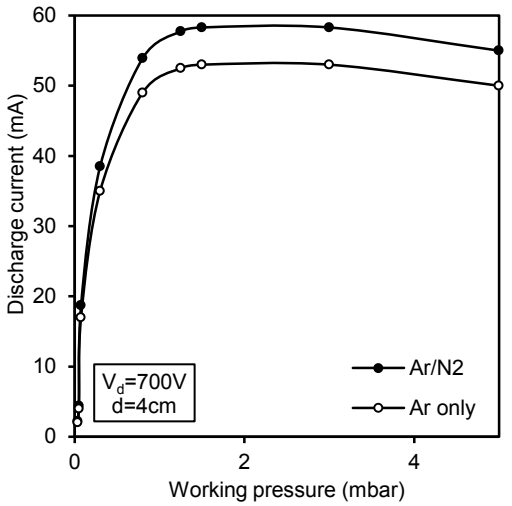

Figure (9) Comparison between current-pressure curves for Ar gas and Ar:N_2 mixture (4:1) at discharge voltage of 700V and inter-electrode distance of 4cm

References

[1] F.F. Chen, Introduction to Plasma Physics and Controlled Fusion, 2nd edition, Plenum Press (NY), p. 22 (1974).

[2] C. O'Leary, Design, Construction and Characterisation of a Variable Balance Magnetron Sputtering System, Department of Electronic Engineering, Dublin City University, Ireland, p. 15 (1999).

[3] T.J. Boyd and J. Sanderson, Physics of Plasmas, Cambridge University Press (2003).

[4] F. Ghaleb and A. Belasri, Numerical and theoretical calculation of breakdown voltage in the electrical discharge, Radiation Effects and Defects in Solids, 1, 1-7 (2012).

[5] M.A. Lieberman and A.J. Lichtenberg, Principles of Plasma Physics and Materials Processing, Second edition, Wiley, p. 547 (2005).

[6] P. Văsina, Plasma diagnostics focused on new magnetron sputtering devices for thin film deposition, PhD thesis, Universit´e Paris-Sud XI, France & Masaryk University in Brno, Czech Republic, pp. 12-19 (2005).

[7] M.M. Mansour, N.M. El-Sayed, O.F. Farag and M.H. Elghazaly, Effect of He and Ar Addition on N_2 Glow Discharge Characteristics and Plasma Diagnostics, Arab J. of Nuclear Sci. and Applications, 46(1), 116-125 (2013).

[8] I. Svadkovski, D. Golosov and S. Zavatskiy, Characterisation parameters for unbalanced magnetron sputtering systems, Vacuum, 68, 283–290 (2003).

[9] A.A. Solov'ev, Investigation of Plasma Characteristics in an Unbalanced Magnetron Sputtering System, Plasma Phys. Rep., 35(5), 399–408 (2009).

 ISSN (printed) 1813-2065, (online) 2309-1673 Printed in IRAQ

[10] A. Bojarov, M. Radmilovic-Radjenovic and Z. Petrovic, Effect of the ion induced secondary electron emission on the characteristics of RF plasmas, Publ. Astron. Obs. Belgrade, 89, 131-134 (2010).
[11] J. Goree and T. E. Sheridan, Magnetic field dependence of sputtering magnetron efficiency, Appl. Phys. Lett., 59(9), 1052-1054 (1991).
[12] J.W. Bradley, Measurements of the sheath potential in low density plasmas, J. Phys. D: Appl. Phys., 25, 1443-1453 (1992).
[13] M.B. Hendricks, Effects of ion-induced electron emission on magnetron plasma instabilities, J. Vac. Sci. Technol. A 12, 1408 (1994)
[14] T.E. Sheridan, M.J. Goeckner and J. Goree, Electron velocity distribution functions in a sputtering magnetron discharge for the ExB direction, J. Vac. Sci. Technol. A 16(4), 2173-2176 (1998).
[15] R. Arnell and P. Kelly, Recent advances in magnetron sputtering, Surf. Coat. Technol., 112, 170-176 (1999).
[16] P.J. Kelly and R.D. Arnell, Magnetron sputtering: a review of recent developments and applications, Vacuum, 56, 159-172 (2000).
[17] V. Rigato, Effects of plasma non-homogeneity on the physical properties of sputtered thin films, Surf. Coat. Technol., 142-144, 943-949 (2001).
[18] E. Martines, Electrostatic fluctuations in a direct current magnetron sputtering plasma, Phys. of Plasmas, 8(6), 3042-3050 (2001).
[19] Annemie Bogaerts, Gas discharge plasmas and their applications (Review), Spectrochimica Acta, Part B57, 609–658 (2002).
[20] C.H. Shon and J.K. Lee, Modeling of Magnetron Sputtering Plasmas, Appl. Surf. Sci., 192, 258-269 (2002).
[21] I. Levchenko, Stable plasma configurations in a cylindrical magnetron discharge, Appl. Phys. Lett., 85(12), 2202-2204 (2004).
[22] G. Petraconi, Longitudinal Magnetic Field Effect on the Electrical Breakdown in Low Pressure Gases, Brazilian J. of Physics, 34(4B), 1662-1666 (2004).
[23] M.H. Elghazaly, S. Solyman and A.M. Abdelbaky, Study of Some Basic Transport Coefficients in Noble-Gas Discharge Plasmas, Egypt. J. Solids, 30(1), 137 (2007).
[24] H. Yasuda, L. Ledernez, F. Olcaytug and G. Urban, Electron dynamics of low-pressure deposition plasma, Pure Appl. Chem, 80(9), 1883-1892 (2008).
[25] M. Yusupov, Behavior of electrons in a dual-magnetron sputter deposition system: a Monte Carlo model, New J. of Physics, 13, 033018 (2011).
[26] M. Yusupov, Elucidating the asymmetric behavior of the discharge in a dual magnetron sputter deposition system, Appl. Phys. Lett., 98, 131502 (2011).
[27] M.A. Hassouba and N. Dawood, Study the Effect of Magnetic Field on the Electrical Characteristics of the Glow Discharge, Adv. in Appl. Sci. Res., 2(4), 123-131 (2011).
[28] E.F. Kotp and A.A. Al-Ojeery, Studies The Effect of Magnetic Field on Argon Plasma Characteristics, Australian J. of Basic and Appl. Sci., 6(3), 817-825 (2012).
[29] Sang-Hun Seo and Hong-Young Chang, Anomalous behaviors of plasma parameters in unbalanced direct-current magnetron discharge, Phys. Plasmas 11, 3595 (2004).
[30] Albert Rauch and André Anders, Estimating electron drift velocities in magnetron discharges, 89, 53-56 (2013).
[31] D.M. Goebel and I. Katz, Basic Plasma Physics (Chapter 3), Fundamentals of Electric Propulsion: Ion and Hall Thrusters, John Wiley & Sons, p. 80 (2008).
[32] Sadik C. Esener, The Future of Data Storage Technologies, Panel report International Technology Research Institute(Maryland, USA), p. 131, 163 (June 1999).

